Available online at www.sciencedirect.com

jmr&t Journal of Materials Research and Technology

https://www.journals.elsevier.com/journal-of-materials-research-and-technology

Original Article

Enhancing the rate dependent fiber/matrix interfacial resistance of ultra-high-performance cement composites through surface abrasion

*Doo-Yeol Yoo**, *Booki Chun*

Department of Architectural Engineering, Hanyang University, 222 Wangsimni-ro, Seongdong-gu, Seoul, 04763, Republic of Korea

ARTICLE INFO

Article history:
Received 15 April 2020
Accepted 25 June 2020
Available online 16 July 2020

Keywords:
Ultra-high-performance cement composites
Straight steel fiber
Surface treatment
Roughness parameter
Pullout behavior
Rate sensitivity

ABSTRACT

Surface-treated steel fibers were developed for enhancing the dynamic pullout performance from ultra-high-performance cement composites (UHPCC). To this end, three types of straight steel fibers with a smooth surface (plain) and longitudinal and transverse abrasions were prepared and tested in impact loading conditions. Sandpapers with various grits were used to abrade the fiber surface; hence, various surface roughness parameters could be achieved. Test results indicated that the surface of smooth steel fiber became much rougher upon abrading it using the sandpapers. The pullout resistance of the abraded steel fibers from UHPCC was better than that of the smooth fiber from the same matrix under the static and impact loads. Some of the transversely abraded steel fibers demonstrated a slip-hardening response, which has been rarely observed in commercial smooth, straight steel fiber products. Considering the pullout resistance and rate sensitivity, the transversely abraded steel fiber was the most effective reinforcement for UHPCC subjected to high loading rates, and these fibers could achieve approximately three times greater equivalent bond strength than the plain fiber. The static and dynamic bond strengths increased almost linearly with the surface roughness of the fiber, whereas the pullout energy had no apparent relation with the roughness.

1. Introduction

Various deformed steel fibers, e.g., hooked, twisted, half-hooked, and crimped fibers, have been developed to improve the tensile performance of ultra-high-performance cement composites (UHPCC) [1–6]. The hooked-end and twisted steel fibers in UHPCC matrix could show much better pullout resistance than a smooth, straight steel fiber [1,7], which is commercially applied in UHPCC products [8]. In particular, the twisted fiber provided the equivalent bond strength of 47 MPa, which is almost five times greater than that of the straight fiber [7]. A novel half-hooked steel fiber was suggested in order to mitigate excessive mechanical anchorage and stress concentration at the end-hook, and its superior pullout resistance compared with that of the straight fiber was verified [5]. As one of its plastic hinges was removed, its bond strength was observed to be roughly between those of hooked-end and straight steel fibers. Zhang et al. [3] also reported that hooked-end and crimped (or corrugated) steel fibers exhibited superior pullout resistance from the UHPCC matrix compared with a

* *Corresponding author.*
E-mail: dyyoo@hanyang.ac.kr (D. Yoo).

https://doi.org/10.1016/j.jmrt.2020.06.080

straight fiber, but the use of excessively deformed fibers, e.g., highly corrugated steel fiber, is recommended to be limited owing to abrupt fracture. Similarly, most of the previous studies have focused on the development of deformed steel fibers as a novel fiber reinforcement for UHPCC to provide better crack bridging capability.

However, in recent years, Yoo et al. [5] have experimentally observed that some of the developed deformed steel fibers, such as hooked-end and half-hooked steel fibers, resulted in poorer tensile performance of UHPCC compared with the commercial short, straight steel fiber. Furthermore, although the twisted steel fiber provided slightly higher tensile strength for UHPCC composites than the straight one, similar to a previous study [6], a longer straight steel fiber having an identical aspect ratio of 100 exhibited better tensile performance than the twisted fiber at a high volume fraction of 2%. Such a deterioration of the tensile performance of the composites upon using the deformed steel fibers is mainly attributed to the excessive mechanical anchorage effect, non-uniform dispersion of fibers, and high brittleness of the matrix, leading to premature pullout failures. The test results of Murali et al. [4] indicate that the hooked-end steel fiber is more effective in terms of the energy dissipation capacity of the UHPCC than the crimped fiber at various dosages ranging from 0.5% to 2%. The order of effectiveness of deformed steel fibers in enhancing the tensile performance of UHPCC is thus determined to be twisted fiber > hooked-end (or half-hooked) fiber > crimped fiber.

Although the twisted steel fiber is most effective in enhancing the tensile performance of UHPCC among the deformed steel fibers introduced so far, its reinforcing efficiency is even lower than that of the long straight steel fiber [5]. The insufficient reinforcing efficiency of deformed steel fibers for UHPCC composites became more evident at high loading rates, such as impact load [9]. Therefore, a novel promising steel fiber type needs to be developed for improving the tensile performance of UHPCC without geometrical deformation, and it is believed that surface treatment can be one of the solutions. Stengel [10] first adopted a method for roughening the surface of a fiber and indicated that the interfacial bond resistance of the original fiber is greatly enhanced by increasing the surface roughness. Chun et al. [11] also recently reported that abrading the surface of smooth, straight steel fiber is effective in enhancing the pullout resistance from UHPCC under both aligned and inclined conditions under static loads. Therefore, in this study, the newly introduced abraded straight steel fibers are adopted as a reinforcement for UHPCC. An examination of the dynamic pullout behaviors of abraded steel fibers from UHPCC is highly desired, as it is well known that they are widely applied in the military field owing to their excellent resistance to extreme loads, such as impact. However, to the best of the authors' knowledge, no study on their dynamic pullout behavior has been published yet; thus, it is first investigated in the present study. To this end, the surface of a smooth, straight steel fiber was treated using sandpapers with various grits, ranging from 120 to 800, in both longitudinal and transverse directions. The dynamic pullout behaviors of smooth and abraded steel fibers from UHPCC were then evaluated using an impact test machine, and the surface roughness was analyzed quantitatively using atomic force microscope (AFM) images. Finally, the loading rate sensitivity of the pullout parameters, such as the average bond strength and pullout energy, was investigated.

Table 1 – Chemical compositions of cement and silica fume.

Composition %	Cement[a]	Silica fume
CaO	61.33	0.38
Al_2O_3	6.40	0.25
SiO_2	21.01	96.00
Fe_2O_3	3.12	0.12
MgO	3.02	0.10
SO_3	2.30	–

[a] Type I Portland cement.

2. Test program

2.1. *Specimen preparation*

Various fibers have been considered as one of the most effective reinforcing materials for cement composites [12–14], and among them, steel fiber has been most frequently adopted to UHPCC matrix for decades. The fiber surface was treated using sandpapers with various grits, ranging from 120 to 800, for analyzing the effect of surface roughness on the dynamic pullout behavior of a straight steel fiber from UHPCC matrix. The grit number indicates the number of abrasive particles contained in one square inch of the sandpaper, meaning that the smaller grit has the coarser particle. The surface of steel fibers was roughened by abrading it using the sandpapers in both longitudinal and transverse directions regularly. In order to make the surface rough, the end of steel fiber was tightly grasped using a pincer, and it was then manually abraded through the sandpaper. Subsequently, the rugged fiber surface was confirmed using the scanning electron microscope (SEM) images shown in Fig. 1 and compared with that of a plain steel fiber. By using a sandpaper with a higher grit, a finer surface roughness was observed owing to the smaller abrasive particles on the sandpaper. The roughness pattern was evidently distinguished based on the sanding direction. Stengel [10] similarly adopted sandpapers to abrade polyvinyl alcohol fibers in UHPCC and found a great improvement of the bond strength owing to an increased surface roughness.

For preparing UHPCC matrix, Type I Portland cement and silica fume were adopted as cementitious materials. Their mean particle sizes were approximately 22 μm and 0.31 μm, respectively, and their chemical compositions and physical properties are given in Table 1 [15]. Silica flour with a grain size of 4.2 μm and high silicon dioxide content was used as a filler, whereas silica sand with a grain size of 337 μm was adopted as a fine aggregate. The existence of coarse aggregate negatively affected the flexural strength of ultra-high-performance fiber-reinforced concrete [16], considering the bond performance of steel fibers. Thus, the coarse aggregate was excluded from the mixture, similar to the conventional UHPCC mixture [17,18]. A fairly low water-binder (W/B) ratio of 0.2 was used to achieve excellent compressive strength of the matrix (greater than 150 MPa as per the ACI committee 239 [19]), and a superplasti-

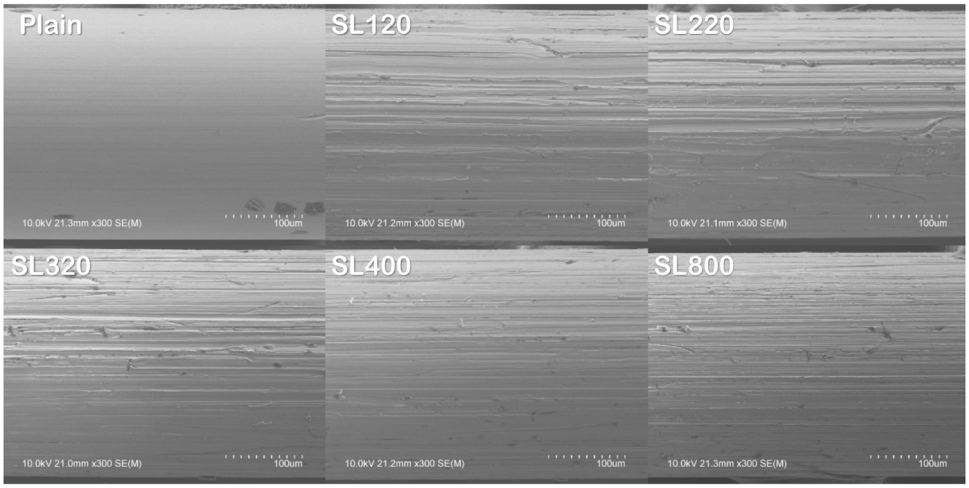

(a)

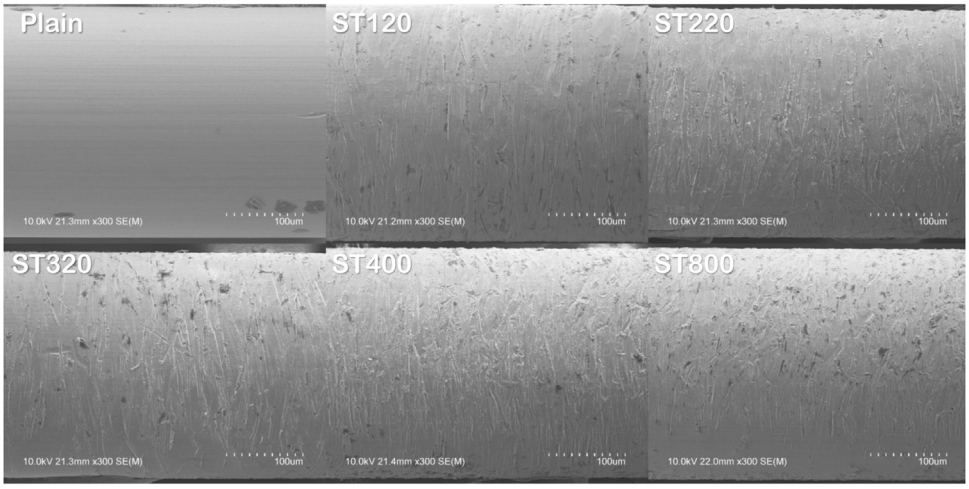

(b)

Fig. 1 – SEM images on the fiber surface: (a) longitudinally sanded fibers and (b) transversely sanded fibers.

Table 2 – Mix proportion of UHPCC.

W/B[b]	Mix design [kg/m^3]					
	Water	Cement	Silica fume	Silica sand	Silica flour	SP[a]
0.2	160.3	788.5	197.1	867.4	236.6	52.6

W/B, water-to-binder ratio; SP, superplasticizer.
[a] Superplasticizer includes 30% solid (=15.8 kg/m^3) and 70% water (=36.8 kg/m^3).
[b] W/B is calculated by dividing total water content by total amount of binder.

cizer with a density of 1.01 g/cm^3 and 30% solid contents was added to have sufficient fluidity. The detailed mix proportion of UHPCC is given in Table 2.

A Hobart mixer was used for mixing the ingredients. All the dry powders, such as cement and silica fume, flour, and sand, were added to the mixer and pre-mixed for 10 min to disperse them homogeneously. Water mixed with the superplasticizer was then added to the mixer and mixed for 10 min more until the mixture became flowable. The degree of flowability of the fresh UHPCC mixture was evaluated using a flow table test with a mini-slump cone in accordance with ASTM C1437 [20], and it was measured to be approximately 250 mm.

A small dog-bone specimen was used for analyzing the pullout behavior of steel fibers from the UHPCC matrix. The schematic description of the dog bone specimen with dimensional information is shown in Fig. 2a. The cross-sectional dimensions of the specimen were 25 × 25 mm^2, and the length was 75 mm. A single steel fiber was fixed at the center of the mold using a very thin PVC sheet and a form board. A shorter embedment length of 10 mm was considered to pull the fiber out from the designed side consistently. The full length of the

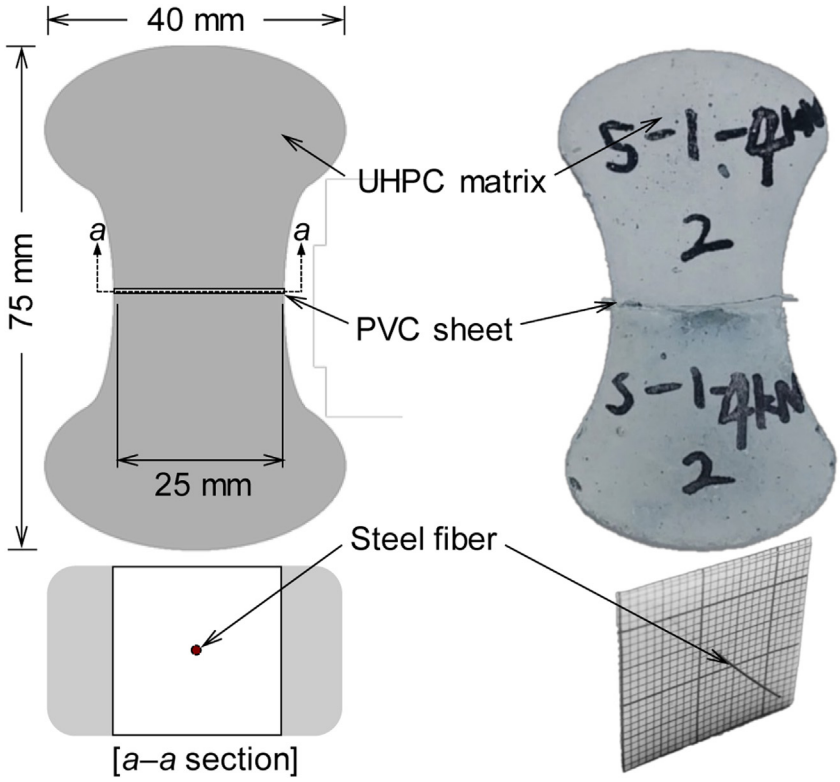

Fig. 2 – Schematic description of dog-bond specimen.

straight steel fiber used was 30 mm, and the geometrical and physical properties of the used plain fiber are summarized in Table 3. At the opposite side, the steel fiber was bent to prevent slipping of the fiber from the matrix. Once the fiber was fixed, the fresh UHPCC mixture was cast into a side of the mold and cured for 24 h at room temperature. Then, the other side of the mold was filled with the fresh mixture and cured for another 24 h before demolding. Subsequently, the dog bone specimens were immersed in a water tank at a high temperature of 90 °C for 48 h to promote strength development, as per the FHWA recommendation [18].

2.2. *Static and impact pullout tests*

Fig. 3a shows the setup for the static pullout test. The prefabricated dog-bone specimen is inserted into the steel grip, and a uniaxial force is applied monotonically at a rate of 0.018 mm/s to pull the fiber out from the matrix. Based on an assumption of negligible elastic deformation of the specimen and the steel grip, the fiber slip was directly measured based on the displacement of the crosshead using a universal testing machine, which is consistent with the test setup from previous studies [21,22]. A load cell was affixed to the crosshead, and its maximum load capacity was 3 kN with a precision of 0.5 N. Two rollers were installed in the steel grip at the contact point between the grip jig and the specimen to allow a slight rotation of the dog bone specimen under the uniaxial load.

The setup for the impact pullout test is illustrated in Fig. 3b. Similar to the static test setup, a dog bone specimen was inserted into the steel grip jig, and a uniaxial load was instantly applied through a piston with increased air pressure. The impact test machine was designed to provide various air pressures ranging from 0.5 kN to 10 kN for various loading rates. An air pressure of 8 kN was applied in this study, which resulted in the loading rate of 4800 mm/s without the specimen. A dynamic load cell was affixed to the testing machine on the side opposite to that of the loading piston to measure the pure impact pullout load, excluding the inertial effect of the specimen. The maximum load capacity and precision of the dynamic load cell used were 9.8 kN and 1.6 N, respectively. Based on the assumption of negligible elastic deformation of the specimen and the grip jig, the fiber slip from UHPCC matrix was directly measured using a potentiometer. The pullout load and displacement data were collected from a dynamic data logger (DEWE-43) at a sampling rate of 20 kHz.

3. Test results and discussion

3.1. *Evaluation of surface roughness*

The surface roughness of the smooth and abraded straight steel fibers was quantitatively evaluated based on the AFM image analysis. Three-dimensional (3-D) images were first obtained from the XE-100 AFM machine with an area of $40 \times 40\,\mu m^2$, and they were downsized to an area of $35 \times 35\,\mu m^2$ to improve the accuracy of image analysis by cutting the edges. As the plain smooth, straight steel fiber has a circular cross-section, it was calibrated using a quadratic function with a high coefficient of determination (R^2) > 0.99. Then, the heights of the abraded fiber surface were calculated after

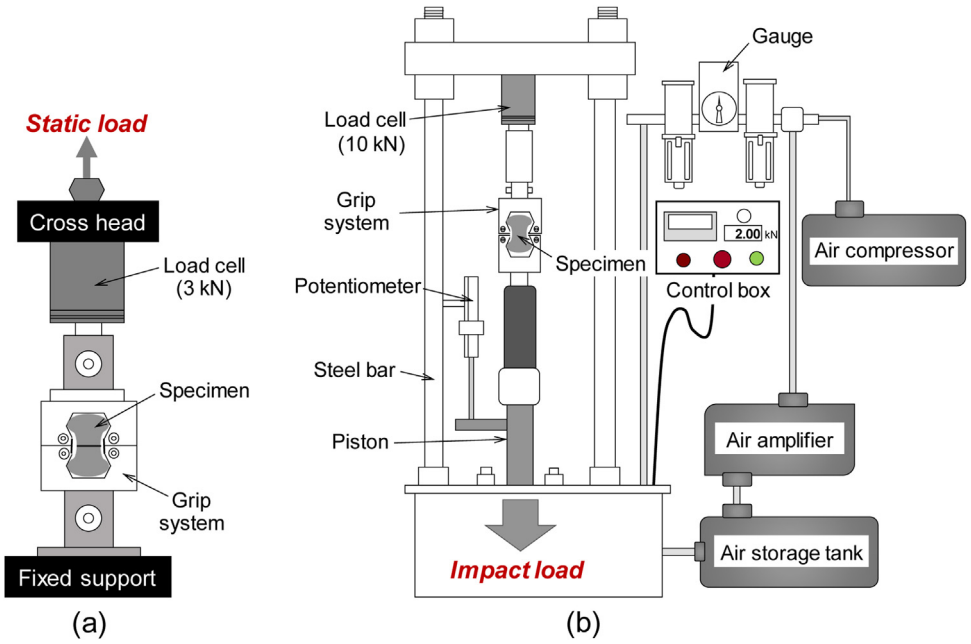

Fig. 3 – Schematic description of (a) static pullout test setup and (b) impact pullout test setup.

Table 3 – Geometrical and physical properties of smooth, straight steel fiber.

Diameter, d_f [mm]	Length, l_f [mm]	Aspect ratio [l_f/d_f]	Density [g/cm^3]	Tensile strength, f_t [MPa]	Elastic modulus, E [GPa]
0.3	30.0	100.0	7.9	2580	200

fitting the images from the quadratic function. The modified AFM images of the fiber surface are shown in Fig. 4.

A surface roughness parameter, R_a, was adopted for quantitative evaluation from Eq. (1), and a mean value of the height profiles was used.

$$Ra = \frac{1}{n}\sum_{i=1}^{n}\left|y_i\right| \tag{1}$$

where n is the number of data used and y_i is the height of the i^{th} point in nanometers.

The calculated roughness values are shown in Fig. 5. It was evident that the surface of the smooth steel fiber became significantly rougher because of the sanding process in both longitudinal and transverse directions. Regardless of the sanding direction, the highest roughness value was observed with the use of the lowest grit of 120, approximately 14.4 times higher than that of the plain fiber (R_a of 27.1 nm). This is because the coarser particles on the sandpaper can excoriate the fiber surface more effectively and deeply. Therefore, by increasing the grit number up to 800, the surface roughness became moderate in general, compared with that of the fibers abraded with a 120-grit sandpaper. The longitudinally abraded fibers showed slightly greater surface roughness values than the counterparts in the transverse direction at identical sandpaper grit numbers: for example, the roughness values of the longitudinal fiber sample were approximately 110% higher than those of the transverse fiber samples on average. As the fiber–matrix interface is densely packed, owing to high-fineness ingredients and hydration products, the smooth, straight steel fiber is scratched, in general, during its pulling out process from the UHPCC matrix [7]. Ranjbarian et al. [23] reported that, during the pulling out process of a synthetic fiber, its surface is peeled off owing to the cement hydrate and filling particles and accumulated at the interface. The peeled off fiber filaments are stacked on the fiber–matrix interface, which may provide a radial pressure to the surrounding matrix, thereby confining the fiber more tightly in reverse. The pre-abraded steel fibers used in this study have abundant steel materials on the surface, and these can be easily peeled off during the pulling out process. Therefore, it is expected that the abraded steel fibers can exhibit higher pullout resistance from the cement matrix than the plain fiber.

3.2. *Static pullout behavior*

The pullout parameters, i.e., the average bond strength, pullout energy, and equivalent bond strength, are calculated using the following equations:

$$\tau_{av} = \frac{P_{max}}{\pi d_f L_E} \tag{2}$$

$$W_P = \int_{S=0}^{S=L_E} P(S)\,dS \tag{3}$$

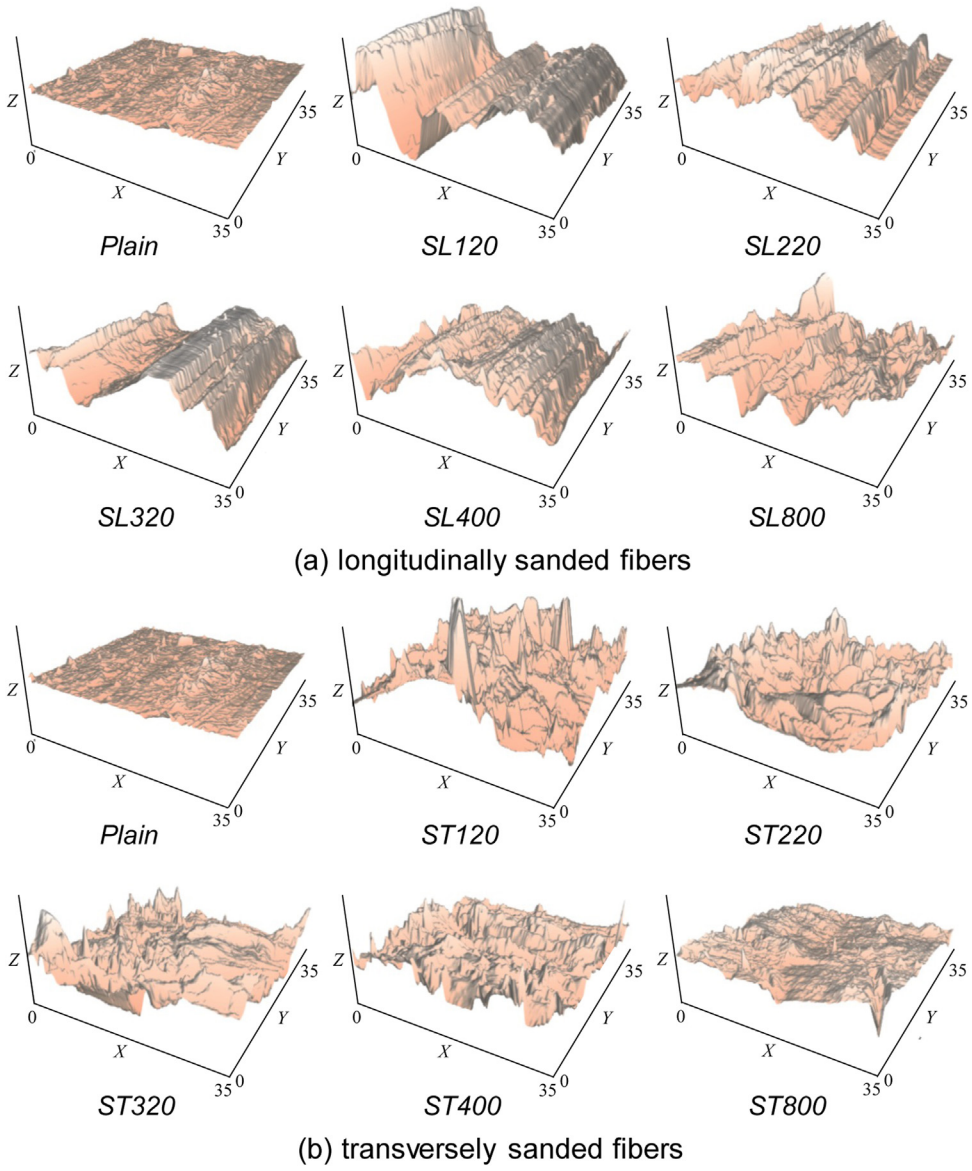

Fig. 4 – Fitted AFM images of surface roughness: (a) longitudinally sanded fibers and (b) transversely sanded fibers.

$$\tau_{eq} = \frac{2W_p}{\pi d_f L_E^2} \tag{4}$$

where τ_{av} is the average bond strength, P_{max} is the maximum pullout load, d_f is the fiber diameter, L_E is the initial embedment length of the fiber, W_P is the pullout energy, S is the fiber end-slip, P(S) is the pullout energy at a certain value of S, and τ_{eq} is the equivalent bond strength.

The average bond stress–slip curves of all the tested samples are shown in Fig. 6, and their pullout parameters are shown in Fig. 7. At least five dog-bone samples were used for each variable to obtain reliable average values. Regardless of the sanding direction, the abraded steel fibers in UHPCC showed higher pullout resistance than the plain fiber, mainly owing to the increased surface roughness. Stengel [10] similarly reported that the roughness of the fiber surface is dependent on the sandpaper grit, and the bond performance of a surface-treated fiber is greatly enhanced compared with that of the original fiber because the bond mechanism at the fiber–matrix interface is influenced by the surface roughness. The bond–slip curves of the sanded fibers in the longitudinal direction exhibited similar shapes to those of the plain fiber, although their bond strength and pullout energy are significantly increased in Fig. 6a. However, the bond–slip curve shapes of the transversely sanded fibers were different from those of the plain fiber. Furthermore, some samples exhibited a slip-hardening response, causing a higher pullout load-carrying capacity after a full debonding of the fiber, which has been rarely observed in the pullout tests of straight steel fibers embedded in the conventional UHPCC matrix [1,7,24]. This is because the abundant steel materials remaining on the fiber surface after the abrasion process with a sandpaper are easily peeled off by the surrounding cement particles and accumulated at the fiber–matrix interface, which continuously increases the frictional shear resistance.

Even though the pullout resistance of the abraded steel fibers from the UHPCC matrix was improved by the sanding process as compared to the plain fiber, their pullout parameters, i.e., the average bond strength and pullout energy, were not noticeably influenced by the sanding direction and sandpaper grit, as shown in Fig. 7. The transversely abraded steel fibers exhibited a re-increase in the pullout load after reaching the initial peak, which was maintained up to large slip values. Such a slip-hardening phenomenon was evident at higher sandpaper grits, e.g., 400 and 800, resulting in highly improved pullout energy absorption capacities, shown in Fig. 7b. For example, the sample ST400 showed the highest pullout energy of 1012 mJ, approximately 241% higher than that (420 mJ) of the plain sample.

Fig. 8a shows the correlation between the surface roughness, R_a, and the average bond strength of the abraded steel fibers in the UHPCC matrix. It was evident that the average bond strength increases with an increase in the surface roughness, R_a, regardless of the sanding direction. This indicates that abrading the steel fiber surface is effective in enhancing its pullout resistance, and the effectiveness increases by making the surface rougher, consistent with the findings of Stengel [10]. On the contrary, no evident correlation between the value of R_a and the pullout energy is observed in Fig. 8b. This might be because, due to the higher bond strength and stacked fiber filaments on the interface, the cement matrix surrounding the fiber became loose once the fiber started to be pulled out from the matrix after a full debonding that resulted in a steeper decrease of the post-peak pullout load with the slip. Therefore, it is recommended that 1) the fiber surface should be made rougher to improve the bond strength of the straight steel fiber in the UHPCC matrix, and 2) the transverse sanding process using a sandpaper with higher grits is preferential to demonstrate a slip-hardening response.

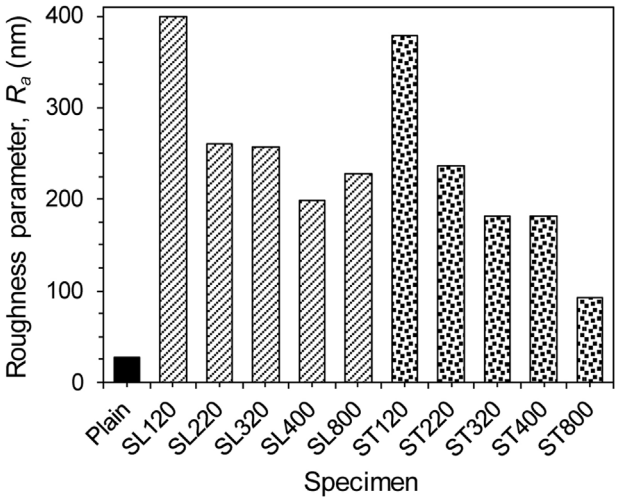

Fig. 5 – Summary of roughness parameter.

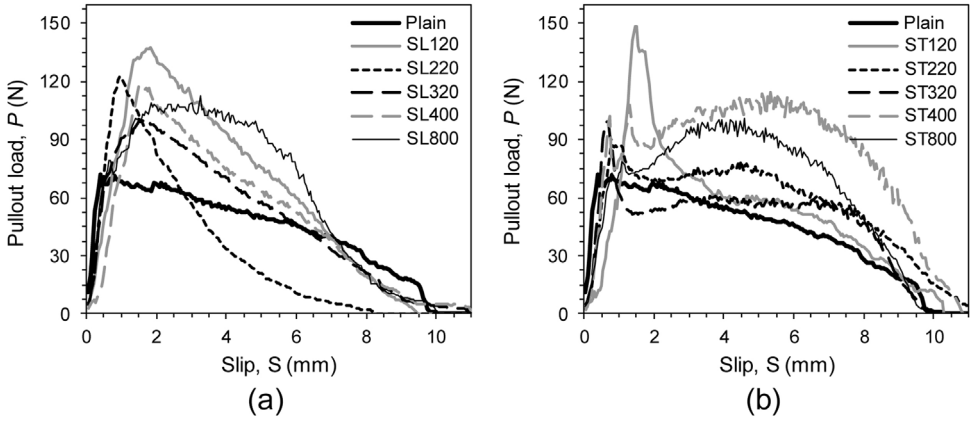

Fig. 6 – Static pullout load versus slip curves: (a) longitudinally sanded fiber samples and (b) transversely sanded fiber samples.

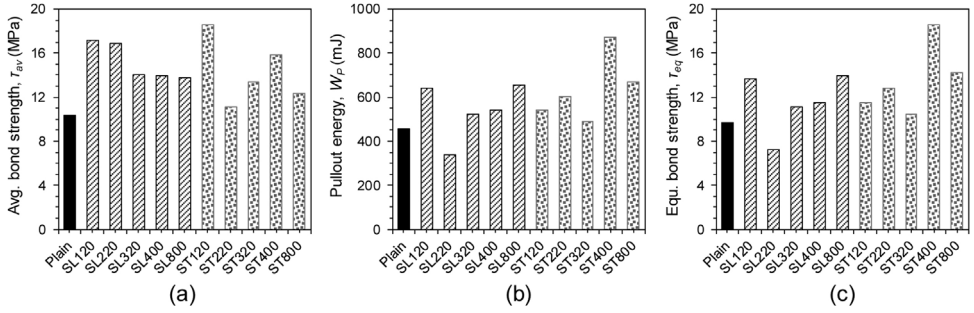

Fig. 7 – Summary of static pullout parameters: (a) average bond strength, (b) pullout energy, and (c) equivalent bond strength.

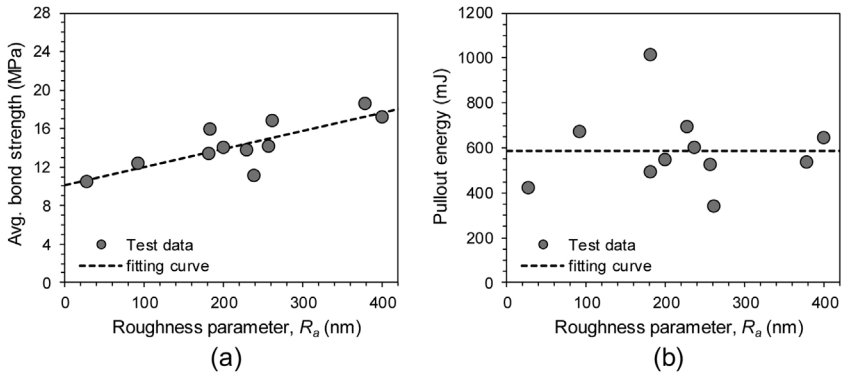

Fig. 8 – Correlation between the static pullout parameters and roughness parameter: (a) average bond strength and (b) pullout energy.

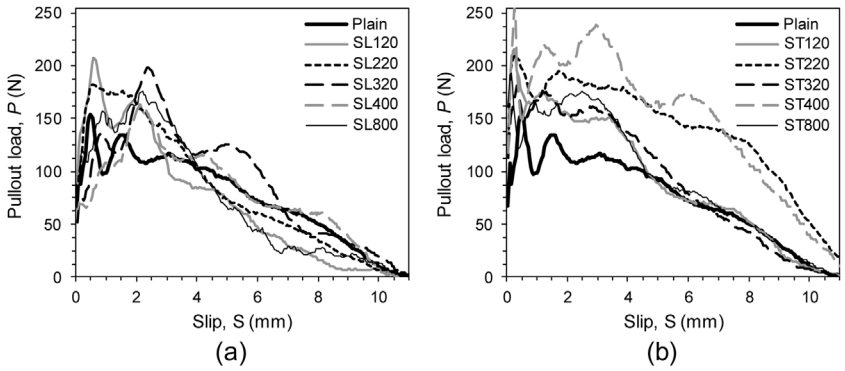

Fig. 9 – Dynamic pullout load versus slip curves: (a) longitudinally sanded fiber samples and (b) transversely sanded fiber samples.

3.3. *Impact pullout behavior*

The average pullout load–slip curves of all the tested samples under impact loads are shown in Fig. 9, and their impact pullout parameters are summarized in Fig. 10. Owing to an instant application of load and vibrations of the sample and test instrumentation, fluctuated pullout load–slip curves were recorded. A similar phenomenon has been reported by several studies [25,26]. Although the data became fluctuated under the impact load, the global load–slip curve shapes were similar to those under the static load. The slip-hardening response, which was observed in some of the transversely sanded fiber samples, became vague at the impact, consistent with the change from the deflection-hardening response under the static load to the deflection-softening response under the impact load [27]. The pullout resistance of both the plain and abraded steel fibers from UHPCC was improved under the impact load, owing to the increased loading rate. The average loading rate under the impact pullout loads was observed to be approximately 420 mm/s, which is much greater than that under the static loading condition that is 0.018 mm/s. The average bond strengths of the plain (P), longitudinal (SL), and transverse (ST) abraded steel fibers were observed to be 16.6 MPa, 20.6 MPa, and 24.8 MPa on average, respectively, under the impact loads. The rate-sensitive pullout behavior of smooth, straight steel fibers from UHPCC has been reported by Tai et al. [2] and Yoo et al. [28]. Consistently, the average bond strengths of the plain, longitudinally abraded, and transversely abraded steel fibers tested in this study were also improved by approximately 159%, 136%, and 174%, respectively, under the impact loading conditions. Similar to the static pullout test results, the abraded steel fiber samples showed better pullout resistance than the plain fiber, in terms of the bond strengths and pullout energy in Fig. 10 in general. It is thus concluded that sanding the fiber surface is effective in enhancing the pullout resistance under both the static and impact loading conditions. However, the effectiveness of sanding the surface of smooth fibers was mitigated by increasing the loading rate, especially for the longitudinal samples. For instance, the static bond strength of plain fiber in UHPCC increased by as much as 145% owing to sanding in the longitudinal direction, whereas it increased only by 123% under the impact loads on average. This is consistent with the findings of Yoo et al. [28], who reported that a smooth, straight steel fiber in a UHPCC matrix is most sensitive to the loading rate, followed by half-hooked and twisted steel fibers in the same matrix, owing to premature failures of the surrounding matrix, known as spalling, or fibers. In contrast, the magnitude of improvement of the bond strength of the transversely sanded fiber samples was higher than that of the plain fiber sample, indicating higher rate sensitivity. As shown in Fig. 10, the dynamic bond strengths and pullout energy of the plain steel fiber from the UHPCC matrix were improved by abrading its surface. The transversely sanded fiber samples

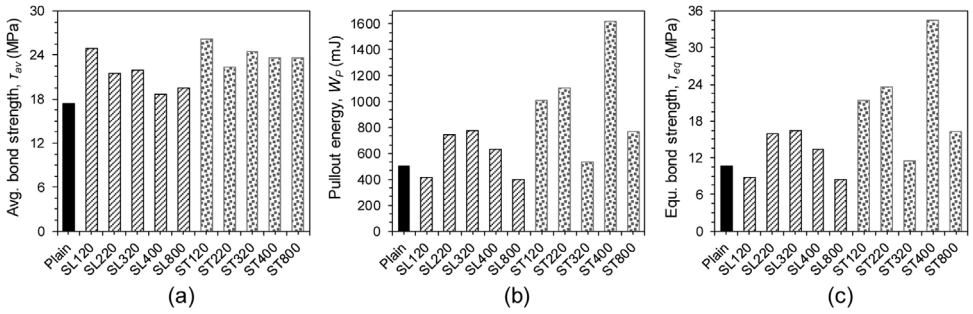

Fig. 10 – Summary of dynamic pullout parameters: (a) average bond strength, (b) pullout energy, and (c) equivalent bond strength.

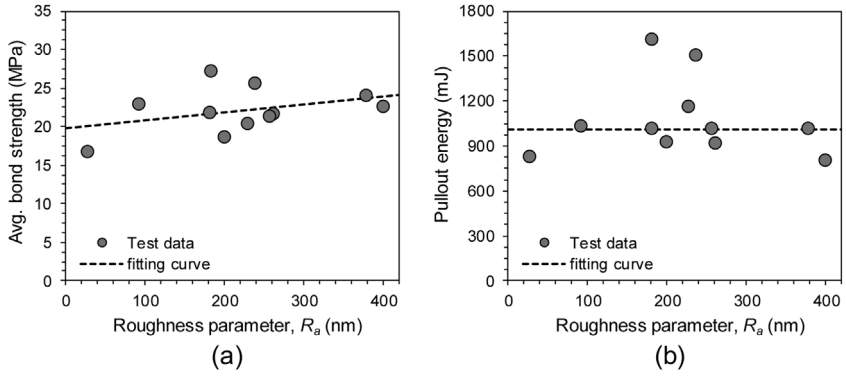

Fig. 11 – Correlation between the dynamic pullout parameters and roughness parameter: (a) average bond strength and (b) pullout energy.

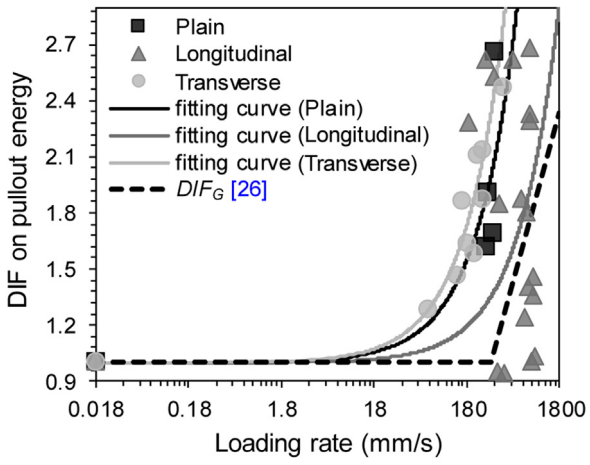

Fig. 12 – DIF and loading rate curves on the pullout energy.

exhibited higher bond strengths and pullout energy than their counterparts sanded in the longitudinal direction or plain ones. The highest average bond strength, pullout energy, and equivalent bond strength obtained were 27.2 MPa, 1605 mJ, and 34.5 MPa, respectively, for the ST400 sample. This indicates that the transversely sanded fiber is preferential to enhance the dynamic pullout resistance than the fiber sanded in the longitudinal direction.

The relationship between the roughness value, R_a, and the dynamic bond strength and pullout energy is shown in Fig. 11 to analyze the effect of roughened surface on the dynamic pullout resistance of the straight steel fiber in UHPCC. The dynamic bond strength increased with an increase in the surface roughness in general, which is consistent with the findings from the static pullout tests, although the degree of correlation, determined based on the coefficient of determination, was relatively low. The enhanced dynamic pullout resistance of the abraded steel fibers might also be due to the peeled off and stacked fiber filaments on the interface. In contrast, there is no apparent relationship between the value of R_a and the dynamic pullout energy in Fig. 11b, although the pullout energies of the abraded fiber samples were higher than those of the plain fiber. Their dynamic pullout energy was slightly reduced by increasing the surface roughness, owing to the loose fiber tunnel, which is similar to the static test results. Synthetically abrading the surface of a steel fiber can be considered an effective way to improve its static and dynamic pullout resistance from the UHPCC matrix.

3.4. *Rate sensitivity*

The loading rate sensitivity is a critical factor for determining an appropriate type of reinforcement for concrete subjected to dynamic and extreme loads, such as earthquake, impact, and blast. The loading rate sensitivity can be analyzed from the dynamic increase factor (DIF) versus loading rate relations, as illustrated in Fig. 12. There was an apparent rate sensitivity of the bond strengths of the plain and abraded steel

fibers from UHPCC: a higher bond strength is achieved at a faster loading rate. This indicates that the steel fibers can more strongly bridge the cracks under the high loading rates. It is effective to use a steel fiber type having a higher loading rate sensitivity as a reinforcement for UHPCC subjected to extreme loads, as it improves the dynamic resistance. Compared with the plain fiber samples, the transversely sanded fibers showed higher rate sensitivity, whereas the longitudinally sanded fiber samples showed lower rate sensitivity. The highest DIF for the average bond strength of the steel fibers in UHPCC was observed to be approximately 2.6 up to the maximum loading rate of approximately 897 mm/s. Similar to the bond strength results, the pullout energy of the plain and abraded steel fibers in UHPCC increased with an increase in the loading rate. Furthermore, the transversely sanded fiber samples exhibited the highest rate sensitivity, followed by the plain and longitudinally sanded fibers. The rate sensitivity difference between the plain and transversely sanded fibers was smaller in the case of pullout energy as compared with that of bond strength, because the slip-hardening response of the latter was mitigated at high loading rates (Figs. 6b and 9b). The order of effectiveness as a reinforcement for UHPCC subjected to impact loads is determined as follows: transversely sanded fiber > plain fiber > longitudinally sanded fiber.

The main role of discontinuous fibers is to bridge the cracks, and the loading rate, indicating a fiber slip rate, is similar to the rate of crack opening in the composites. Thus, the pullout behavior of steel fibers is relevant to the post-cracking tensile behavior of the composites, including the post-cracking tensile strength and fracture energy. Schuler et al. [29] reported that there is a sharp increase in the fracture energy of concrete at high tensile strain rates and proposed the following equation for the relationship between the fracture energy and the crack opening velocity.

$$DIF_G = \frac{G_{fdyn}}{G_{fqs}} = 1,\ \dot{\delta} \le 0.33\,\text{m/s} \tag{5}$$

$$DIF_G = \frac{G_{fdyn}}{G_{fqs}} = A\dot{\delta}^B,\ \dot{\delta} > 0.33\,\text{m/s} \tag{6}$$

where DIF_G is the DIF of the fracture energy, G_{fdyn} is the dynamic fracture energy, G_{fqs} is the quasi-static fracture energy, $\dot{\delta}$ is the crack opening rate, and A and B are constants ($A = 1.74$ and $B = 0.5$).

Under the aligned condition, the pullout energy of the plain and transversely sanded steel fibers in UHPCC were highly sensitive to the loading rate as compared with the fracture energy of concrete, whereas that of the longitudinally sanded fibers was similar or slightly less sensitive to the rate as shown in Fig. 12. This indicates that the reinforcing efficiency of transversely sanded or plain steel fibers on the post-cracking behavior of UHPCC at high loading rates is higher than that of the concrete itself in terms of the energy absorption capacity, if they are well aligned with the direction of the tensile force. Thus, it can be noted that using the transversely sanded or smooth, straight steel fiber as a reinforcement for UHPCC is effective in enhancing its impact resistance.

4. Conclusions

To improve the interfacial bond performance of smooth, straight steel fibers commercially used in the UHPCC matrix, under impact loads, their surface was treated by using sandpapers with various grits in both longitudinal and transverse directions. The surface roughness was quantitatively investigated from the analyses of AFM images, and the impact pullout behaviors of the smooth (plain), longitudinally abraded, and transversely abraded steel fibers from the UHPCC matrix were evaluated. Their rate sensitivity was also analyzed to determine the most appropriate fiber type as a reinforcement for UHPCC subjected to impact loads. From the test results and discussions, the following conclusions can be drawn.

1) The surface of the smooth steel fiber became much rougher by abrading it using a sandpaper in both longitudinal and transverse directions. The coarser particles in the sandpaper deeply excoriated the fiber surface, leading to higher surface roughness. The longitudinally abraded fibers gave slightly higher surface roughness than that of the transverse ones at identical sandpaper grit numbers.
2) The abraded steel fibers exhibited better static pullout resistance from the UHPCC matrix than the plain fiber. The pullout parameters of the abraded steel fibers were not affected by the sandpaper grit and abrading direction. Some of the fibers transversely abraded by using higher sandpaper grits exhibited a slip-hardening response that significantly improved the pullout energy; thus, the pullout energy of the plain fiber increased by as much as 241%.
3) Abrading the fiber surface was also effective in enhancing the dynamic pullout resistance of the plain steel fiber from the UHPCC matrix. Sanding in the transverse direction was preferable to improve the dynamic pullout resistance than sanding in the longitudinal direction. The highest equivalent bond strength of 34.5 MPa was observed in the specimen ST400 at the average loading rate of about 420 mm/s, which is 3.3 times greater than that of plain fiber.
4) Both the static and dynamic bond strengths of the abraded steel fibers in UHPCC increased almost linearly with an increase in the roughness value, R_a, whereas their pullout energies had no apparent relation with the value of R_a.
5) The order of fiber samples in terms of the rate sensitivity of their pullout performance, including the average bond strength and pullout energy, was as follows: transversely sanded fiber > plain fiber > longitudinally sanded fiber. The plain and transversely sanded fibers were also highly sensitive to loading rate as compared to the fracture energy of concrete, indicating their higher reinforcing efficiency.

Conflicts of interest

The authors declare no conflicts of interest.

CRediT authorship contribution statement

Doo-Yeol Yoo: Writing - original draft, Supervision, Formal analysis, Funding acquisition. **Booki Chun:** Conceptualization, Methodology, Data curation, Formal analysis.

Acknowledgement

This research was supported by a Grant (19CTAP-C152069-01) from Technology Advancement Research Program funded by Ministry of Land, Infrastructure and Transport of Korean government.

REFERENCES

[1] Yoo DY, Park JJ, Kim SW. Fiber pullout behavior of HPFRCC: effects of matrix strength and fiber type. Compos Struct 2017;174:263–76.
[2] Tai YS, El-Tawil S, Chung TH. Performance of deformed steel fibers embedded in ultra-high performance concrete subjected to various pullout rates. Cem Concr Res 2016;89:1–13.
[3] Zhang H, Ji T, Lin X. Pullout behavior of steel fibers with different shapes from ultra-high performance concrete (UHPC) prepared with granite powder under different curing conditions. Constr Build Mater 2019;211:688–702.
[4] Murali G, Venkatesh J, Lokesh N, Nava TR, Karthikeyan K. Comparative experimental and analytical modeling of impact energy dissipation of ultra-high performance fibre reinforced concrete. KSCE J Civil Eng 2018;22(8):3112–9.
[5] Yoo DY, Kim S, Kim JJ, Chun B. An experimental study on pullout and tensile behavior of ultra-high-performance concrete reinforced with various steel fibers. Constr Build Mater 2019;206:46–61.
[6] Wille K, Kim DJ, Naaman AE. Strain-hardening UHP-FRC with low fiber contents. Mater Struct 2011;44(3):583–98.
[7] Wille K, Naaman AE. Pullout behavior of high-strength steel fibers embedded in ultra-high-performance concrete. ACI Mater J 2012;09(4):479–87.
[8] Graybeal BA. Flexural behavior of an ultrahigh-performance concrete I-girder. J Bridge Eng 2008;13(6):602–10.
[9] Yoo DY, Banthia N, Lee JY, Yoon YS. Effect of fiber geometric property on rate dependent flexural behavior of ultra-high-performance cementitious composite. Cem Concr Compos 2018;86:57–71.
[10] Stengel T. Effect of surface roughness on the steel fibre bonding in ultra high performance concrete (UHPC). In: Nanotechnology in construction 3. Berlin, Heidelberg: Springer; 2009. p. 371–6.
[11] Chun B, Yoo DY, Banthia N. Achieving slip-hardening behavior of sanded straight steel fibers in ultra-high-performance concrete. Cem Concr Compos 2020, http://dx.doi.org/10.1016/j.cemconcomp.2020.103669, in-press.
[12] Li Z, Wang L, Ma G. Mechanical improvement of continuous steel microcable reinforced geopolymer composites for 3D printing subjected to different loading conditions. Compos Part B-Eng 2020;187:107796.
[13] Farina I, Modano M, Zuccaro G, Goodall R, Colangelo F. Improving flexural strength and toughness of geopolymer mortars through additively manufactured metallic rebars. Compos Part B-Eng 2018;145:155–61.
[14] Farina I, Goodall R, Hernández-Nava E, di Filippo A, Colangelo F, Fraternali F. Design, microstructure and mechanical characterization of Ti6Al4V reinforcing elements for cement composites with fractal architecture. Mater Des 2019;172:107758.
[15] Yoo DY, Kim MJ. High energy absorbent ultra-high-performance concrete with hybrid steel and polyethylene fibers. Constr Build Mater 2019;209:354–63.
[16] Ma J, Orgass M, Dehn F, Schmidt D, Tue NV. Comparative investigations on ultra-high performance concrete with and without coarse aggregates. In: Proceedings International Symposium on Ultra High Performance Concrete (UHPC). 2004.
[17] Richard P, Cheyrezy M. Composition of reactive powder concretes. Cem Concr Res 1995;25(7):1501–11.
[18] Graybeal BA. Material property characterization of ultra-high performance concrete (No. FHWA-HRT-06-103). United States: Federal Highway Administration (FHWA); 2013.
[19] ACI Committee 239. Ultra-high performance concrete. Toronto, Ontario, Canada: ACI Fall Convention; 2012.
[20] ASTM C1437. Standard test method for flow of hydraulic cement mortar. West Conshohocken, PA: ASTM International; 2013. p. 1–2.
[21] Won JP, Hong BT, Lee SJ, Choi SJ. Bonding properties of amorphous micro-steel fibre-reinforced cementitious composites. Compos Struct 2013;102:101–9.
[22] Cao YYY, Yu QL, Brouwers HJH, Chen W. Predicting the rate effects on hooked-end fiber pullout performance from Ultra-High Performance Concrete (UHPC). Cem Concr Res 2019;120:164–75.
[23] Ranjbarian M, Mechtcherine V, Zhang Z, Curosu I, Storm J, Kaliske M. Locking Front Model for pull-out behaviour of PVA microfibre embedded in cementitious matrix. Cem Concr Compos 2019;103:318–30.
[24] Lee Y, Kang ST, Kim JK. Pullout behavior of inclined steel fiber in an ultra-high strength cementitious matrix. Constr Build Mater 2010;24(10):2030–41.
[25] Bindiganavile V, Banthia N. Polymer and steel fiber-reinforced cementitious composites under impact loading – Part 1: bond-slip response. ACI Mater J 2001;98(1):10–6.
[26] Bindiganavile V, Banthia N. Impact response of the fiber-matrix bond in concrete. Can J Civil Eng 2005;32(5):924–33.
[27] Yoo DY, Banthia N, Kang ST, Yoon YS. Effect of fiber orientation on the rate-dependent flexural behavior of ultra-high-performance fiber-reinforced concrete. Compos Struct 2016;157:62–70.
[28] Yoo DY, Kim JJ, Chun B. Dynamic pullout behavior of half-hooked and twisted steel fibers in ultra-high-performance concrete containing expansive agents. Compos Part B: Eng 2019;167:517–32.
[29] Schuler H, Mayrhofer C, Thoma K. Spall experiments for the measurement of the tensile strength and fracture energy of concrete at high strain rates. Int J Impact Eng 2006;32(10):1635–50.